Mapping understory invasive plant species with field and remotely sensed data in Chitwan, Nepal

Jie Dai[a,b,c,*], Dar A. Roberts[b], Doug A. Stow[a,c], Li An[a,c], Sharon J. Hall[d], Scott T. Yabiku[e], Phaedon C. Kyriakidis[b,f]

[a] Department of Geography, San Diego State University, San Diego, CA 92182, USA
[b] Department of Geography, University of California, Santa Barbara, CA 93106, USA
[c] Center for Complex Human-Environment Systems, San Diego State University, San Diego, CA 92182, USA
[d] School of Life Sciences, Arizona State University, Tempe, AZ 85281, USA
[e] Department of Sociology and Criminology, Pennsylvania State University, University Park, PA 16802, USA
[f] Department of Civil Engineering and Geomatics, Cyprus University of Technology, 3036 Limassol, Cyprus

ARTICLE INFO

ABSTRACT

Monitoring invasive species distribution and prevalence is important, but direct field-based assessment is often impractical. In this paper, we introduce and validate a cost-effective method for mapping understory invasive plant species. We utilized Landsat imagery, spectral mixture analysis (SMA) and a maximum entropy (Maxent) modeling framework to map the spatial extent of *Mikania micrantha* in Chitwan National Park, Nepal and community forests within its buffer zone. We developed a spectral library from reference and image sources and applied multiple endmember SMA (MESMA) to selected Landsat imagery. Incorporating the resultant green vegetation and shade fractions into Maxent, we mapped the distribution of understory *M. micrantha* in the study area, with training and testing Area under Curve (AUC) values around 0.80, and kappa around 0.55. In vegetated places, especially mature forests, an increase in green vegetation fraction and decrease in shade fraction was associated with higher likelihood of *M. micrantha* presence. In addition, the inclusion of elevation as a model input further improved map accuracy (AUC around 0.95; kappa around 0.80). Elevation, a surrogate for distance to water in this case, proved to be the determining factor of *M. micrantha*'s distribution in the study area. The combination of MESMA and Maxent can provide significant opportunities for understanding understory vegetation distribution, and contribute to ecological restoration, biodiversity conservation, and provision of sustainable ecosystem services in protected areas.

1. Introduction

Invasive species have long been associated with human-introduced environmental change, rendering negative effects on ecosystem services and human well-being (Pejchar and Mooney, 2009). The first step in invasive species management and intervention requires identifying their geographical locations. Traditional invasive plant detection and identification usually involves intensive field surveys, which can be time consuming and expensive. Remote sensing provides a potential alternative method for detection. In general, direct remote sensing of invasive plants aims to detect spectral, textural and/or phenological differences between the invasive and native species (Bradley, 2014). Spectral differentiation focuses on the unique spectral signatures of invasive plants compared to native vegetation and is mostly applied to

hyperspectral imagery (Asner et al., 2008; Barbosa et al., 2016; Underwood et al., 2003). Textural differentiation examines the distinct spatial patterns of invasive species and background land covers captured within a neighborhood of adjacent pixels and is usually conducted with high-spatial resolution imagery, depending on the size of the invasive plant or its aggregation (Lishawa et al., 2013; McCormick, 1999; Pearlstine et al., 2005). Phenological differentiation identifies different seasonal or inter-annual growth patterns between invasive and native plants, including base and maximum level greenness of growing season, time and rate of greening up and senescence, date of the middle of the season, and other parameters (Bradley et al., 2018; Hoyos et al., 2010; Peterson, 2005; Somers and Asner, 2013). Phenological differentiation requires repeat imaging to gain adequate temporal information to define spectral differences.

Obscured by the top canopy, detection of understory invasive plants is even more challenging, especially in closed-canopy mature forests. Direct detection through passive optical remote sensing techniques can be achieved when understory vegetation has distinct phenologies from overstory species, such as an extended green season or earlier greening up when the overstory trees are leaf-off (Taylor et al., 2013; Tuanmu et al., 2010; Wilfong et al., 2009). Understory invasive plants may be indirectly identified if the invasion introduces competition for nutrients as well as water and renders biochemical changes in overstory leaves, thus altering the spectral features of the overstory vegetation (Asner and Vitousek, 2005). Indirect detection of understory invasive plants may also be achieved through linking its presence with remote sensing imagery related biophysical and socio-ecological factors governing its growth, such as light-availability and human disturbance in the forests (Joshi et al., 2006).

Spectral mixture analysis (SMA) is a powerful tool for inspecting mixed pixels in remote sensing imagery and quantifying their constituents, especially for moderate and coarse spatial resolution images. Theoretically, the invasion of understory plants can introduce changes to the types and quantities of constituents within mixed pixels, which may be directly or indirectly detected in SMA. Nevertheless, few studies have incorporated SMA to investigate understory invasive plant mapping. In this research, we explore the detection and mapping of understory invasive plant species through multiple endmember SMA (MESMA; Roberts et al., 1998) and maximum entropy (Maxent; Phillips et al., 2006) modeling framework. In particular, we map the spatial extent of *Mikania micrantha* in Chitwan National Park (CNP), Nepal and its buffer zone community forests. *M. micrantha* is one of the world's most notorious invaders (IUCN, 2019) and its invasion is jeopardizing and has the potential of totally disrupting local coupled human and natural systems. *M. micrantha* also decreases forest productivity by hindering the growth of native species, weakens social organizations that manage and shape households' resource use in the community forests, and downgrades local ecosystems and their corresponding services (Murphy et al., 2013). According to research literature, and discussions with local forest users and park rangers, *M. micrantha* mostly flourishes in riverine habitats and tends not to grow in higher-elevation environments (Murphy et al., 2013). Given this general distribution pattern, our goal is to create a detailed, pixel-based distribution map for *M. micrantha* in the study area. The results from this research will help identify the locations of *M. micrantha* and guide local invasive plant species management and intervention practices.

2. Methods

2.1. Study area

The Chitwan district is located in the central part of Nepal near the border with India. It is famous for the Chitwan National Park, recognized as a World Heritage site and a significant biodiversity hotspot in the Terai region of Nepal with elevation between 120 and 815 m, nurturing endangered great one-horned rhinoceros (*Rhinoceros unicornis*), Bengal tiger (*Panthera tigris tigris*) and other endemic species (UNESCO, 2019; CEPF, 2019). Chitwan is also home to about 600,000 people who live and farm nearby (Central Bureau of Statistics-Nepal, 2011). Beginning in the 1950s, large-scale deforestation occurred as forest was converted to farmland, and to better manage remaining forests in the area, community forests were established upon passing of the Community Forestry Act in 1993 (Nagendra, 2002; Spiteri and Nepal, 2008). Community forestry programs grant local users limited access to the forest resources and a certain degree of autonomous management (Charnley and Poe, 2007). Our investigation focuses on the Chitwan National Park, established in 1973, and the community forests within its buffer zone (Fig. 1).

The study area has a tropical monsoon climate with mean annual precipitation of 2100 mm with most of the rain falling from June through early October. Average daily temperature ranges from 36 °C in the summer to 18 °C in January. The dominant vegetation types within the park are Sal forests (*Shorea robusta*), riverine mixed forests (most common species include *Acacia catechu, Bombax cieba, Dalbergia sissoo, Maesa chisia, Melia azedarach* and *Trewia nudiflor*) and riparian grasslands (most common species include *Saccharum spontaneum, Narenga porphyracorma, Phragmites karka* and *Imperata cylindraica*).

2.2. Field vegetation inventory

In the three consecutive years of 2013, 2014 and 2015, field vegetation surveys were conducted in the western Chitwan buffer zone community forests, bounded to the south by the Rapti River and the west by the Narayani River (Fig. 2). Field data were collected around the peak biomass period right after the monsoon season, approximately between late September and mid-November. In every community forest, we set up parallel transects that are 200 m apart, angling from human settlements toward the park. Along each transect, at 50 m intervals, we set up a sample site with two 5 m by 5 m plots adjacent to each other and perpendicular to the transect. For each plot, several ecological measurements were obtained, including *M. micrantha* coverage (in categories 0–4 through visual estimation, where 0 represents absence of *M. micrantha*, 1 for 1%–25% coverage and 2 for 26%–50% coverage, etc.), canopy cover (in percentage, measured through a forest densiometer) and identification of dominant tree and herbaceous species.

In the field vegetation survey, the coverage of sample sites in the community forests was affected by accessibility (rivers, lakes and wetlands were inaccessible) and occasionally by likely presence of dangerous animals such as tigers and rhinos. We were able to investigate most of the areas to the north of the Rapti River and to the south of the Narayani River (e.g. in BELS, SAYU, NARA, DIYA, MAJH, SIDD and SETI; Fig. 3). We also crossed the borders of three Sal community forests in the east (e.g. BAND, NABA and DASH; Fig. 3) and doubled the lengths of the sampling transects.

2.3. Ground reference spectra

In September 2018, apart from the field vegetation surveys, we collected in situ reference spectra for major herbaceous species (including *M. micrantha*) at 1 m height with a nadir view geometry under cloud-free conditions within 2 h of solar noon in the community forests. We also collected spectra of other common land cover types in the study area, including soil, non-photosynthetic vegetation (NPV; e.g. senesced grass, plant residue, etc.; Roberts et al., 1993) and gravel fields (categorized as Soil here) in the study area. Spectroscopic surface reflectance data were collected with an Analytical Spectral Devices (ASD) Field-Spec® 4 Standard-Res spectroradiometer (Malvern Panalytical, Westborough, MA). Equipped with three detectors spanning the visible and near infrared (VNIR) and shortwave infrared (SWIR1 and SWIR2), the instrument samples at a spectral range of 350–2500 nm, with a sampling interval of 1.4 nm for the VNIR detector, and 1.1 nm for SWIR detectors. The Full Width Half Maximum is 3 nm in VNIR and 10 nm in the SWIR. With a 25° field of view, the 1.5 m fiber optic cable transmits light from the aperture to the spectrometer. Each plant spectrum was sampled 10 times to account for random errors, and was bracketed by measurements from a Spectralon white reference panel to offset any changes in solar illumination or changes due to weather. The reflectance values, automatically calibrated from the radiance records in the field, were later extracted through the software package ViewSpecPro (Malvern Panalytical, Westborough, MA).

2.4. Remotely sensed data

We obtained Landsat Operational Land Imager (OLI) surface reflectance products (Level-2) from USGS EarthExplorer (https://
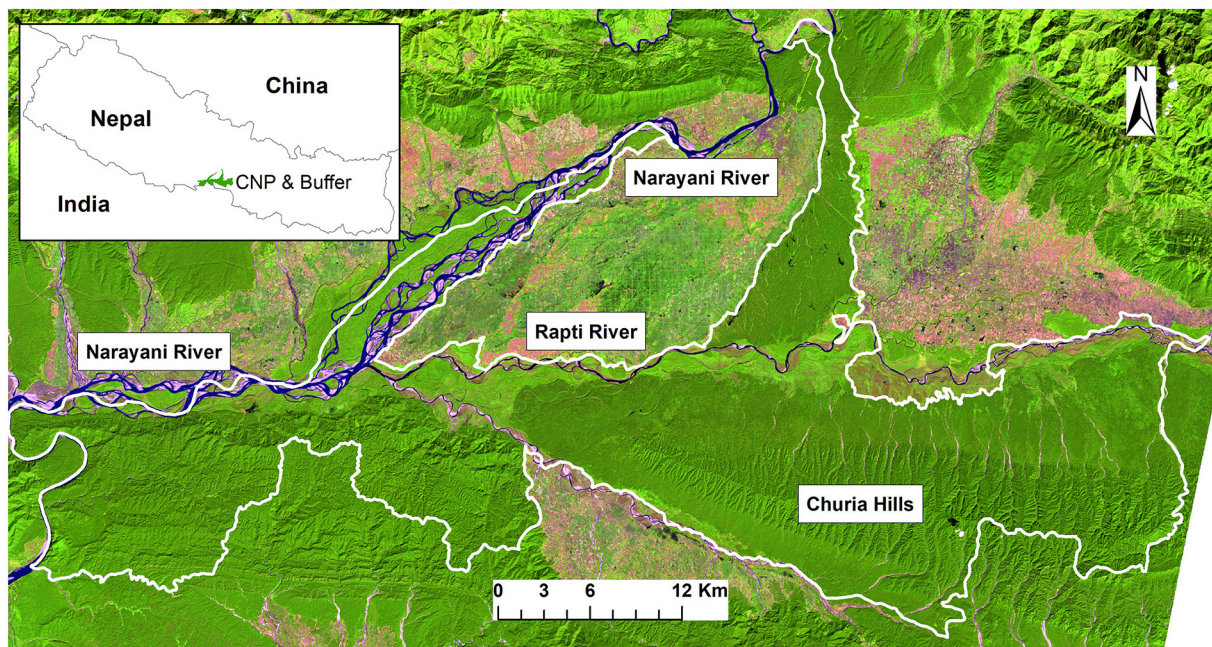
Fig. 1. False colour Landsat 8 three-band composite of the study area (highlighted in white polygon). Image acquisition date: 27 October 2014. Red: Band 6 (1560–1660 nm); Green: Band 5 (845–885 nm); Blue: Band 4 (630–680 nm). (For interpretation of the references to colour in this figure legend, the reader is referred to the web version of this article.)
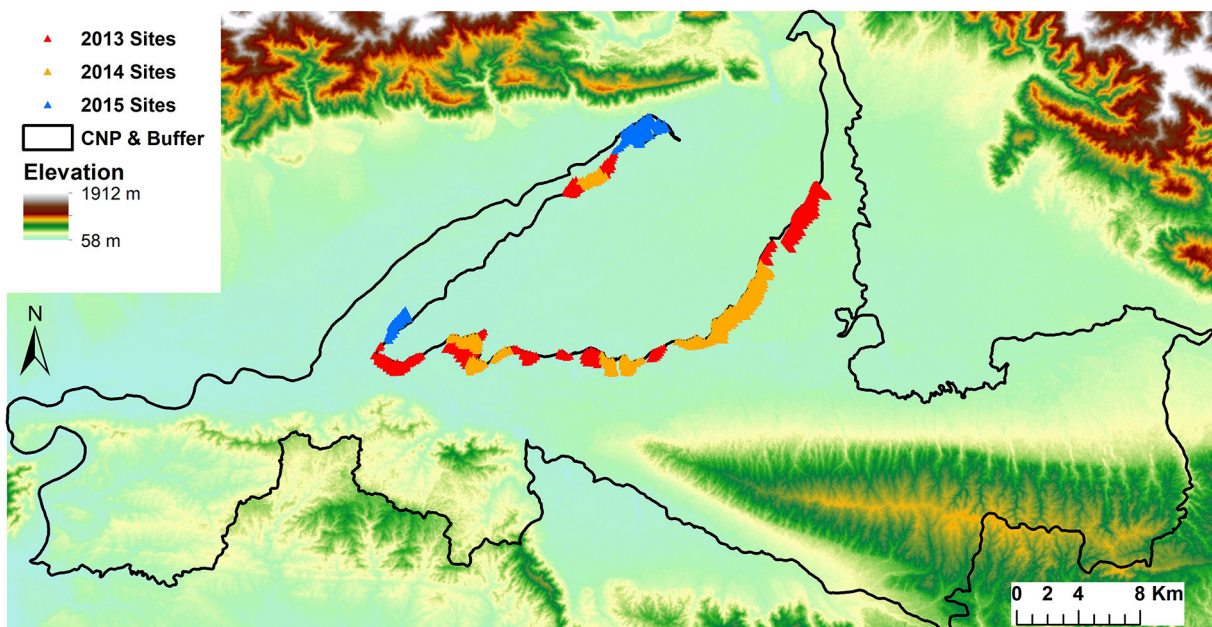

Fig. 2. Terrain map of the study area and vegetation survey sites.

earthexplorer.usgs.gov/) to align with the field vegetation survey dates. For the years 2013, 2014 and 2015, we were able to identify one desirable scene for each year (Path/Row: 142/41; Table 1). We also obtained a 30 m spatial resolution digital elevation model (DEM) derived from Terra Advanced Spaceborne Thermal emission and Reflectance Radiometer (ASTER) stereoscopic imagery for the study area (NASA/METI, 2019).

2.5. Multiple endmember spectral mixture analysis

Spectral mixture analysis (SMA) is a classic method for estimating mixed constituents within ground resolution elements associated with image pixels. It assumes that the spectral reflectance of a pixel can be modeled as the weighted sum of endmember reflectance, or spectrally "pure" materials, within that pixel. Most SMA adopts a linear addition method and the weights correspond to fractions of endmembers in the pixel. As an extension of simple SMA, Multiple Endmember SMA (MESMA) allows the number and types of endmembers to vary on a per-pixel basis, generating more legitimate unmixing results for imagery with high inter- and intra-endmember variance (Roberts et al., 1998).

To apply MESMA, we developed a spectral library across endmember types while incorporating endmember variability. Ground reference spectra, including Green Vegetation (GV), NPV and Soil, were acquired through in situ measurements. Complimentary NPV and Soil
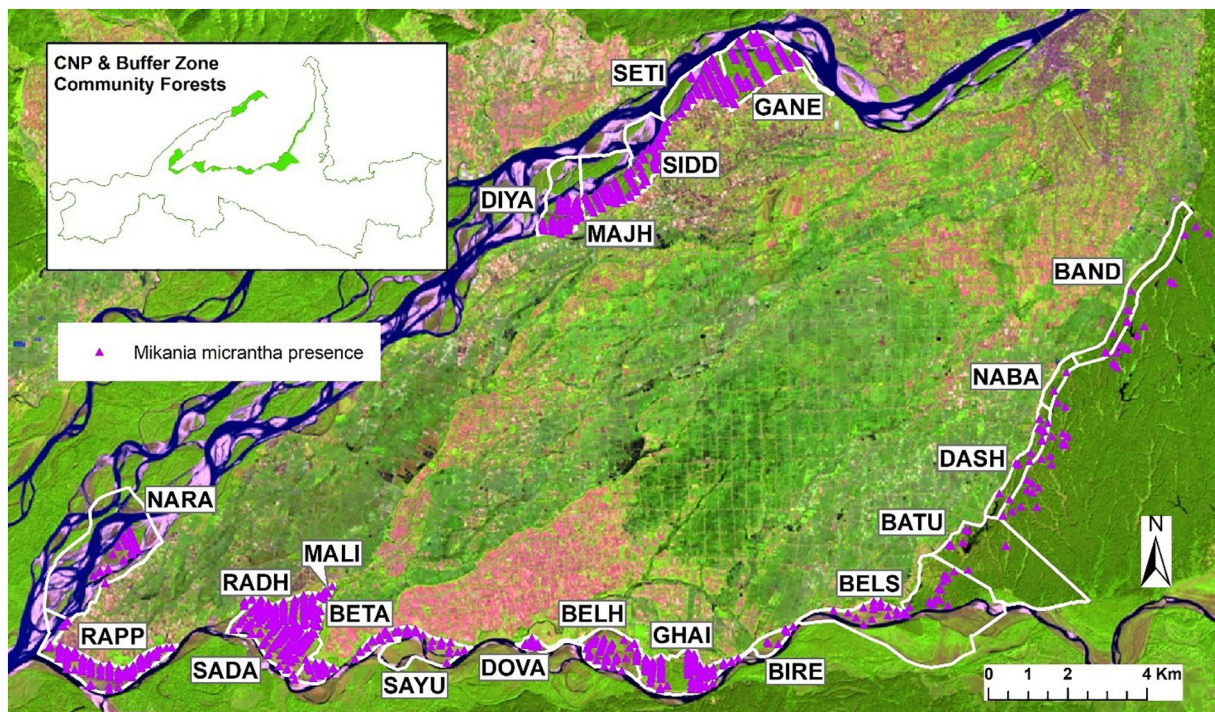
Fig. 3. Community forests (highlighted by white polygons) in the study area and sample sites with *M. micrantha* presence. Background image: false colour Landsat 8 three-band composite. Image acquisition date: 27 October 2014. Red: Band 6 (1560–1660 nm); Green: Band 5 (845–885 nm); Blue: Band 4 (630–680 nm). (For interpretation of the references to colour in this figure legend, the reader is referred to the web version of this article.)

Table 1
Selected Landsat OLI imagery.

Year	Acquisition date	Cloud cover	Image quality
2013	11/09	2.00%	9
2014	10/27	0.94%	9
2015	10/14	4.84%	9

Table 2
Allowed models by endmember types with total model numbers in parentheses.

Two-endmember (7)	Three-endmember (16)	Four-endmember (12)
GV + Shade	GV + NPV + Shade	GV + NPV + Soil + Shade
NPV + Shade	GV + Soil + Shade	
Soil + Shade	NPV + Soil + Shade	

Table 3
Number of total sample sites and invaded sites in each community forest.

Region	Forest code	Total sites	Invaded sites	Invasion %
East Sal	BAND	299	23	7.7%
	NABA	39	4	10.3%
	DASH	232	31	13.4%
	BATU	126	7	5.6%
South Central Rapti	BELS	167	33	19.8%
	BIRE	28	7	25.0%
	GHAI	136	100	73.5%
	BELH	87	39	44.8%
	DOVA	19	10	52.6%
South West Rapti	SAYU	52	21	40.4%
	BETA	109	62	56.9%
	MALI	9	9	100.0%
	RADH	76	76	100.0%
	SADA	177	147	83.1%
Far West	RAPP	148	101	68.2%
	NARA	88	33	37.5%
North Narayani	DIYA	70	62	88.6%
	MAJH	74	67	90.5%
	SIDD	59	47	79.7%
	SETI	92	78	84.8%
	GANE	136	99	72.8%

spectra were identified from two online spectral libraries: (1) Jet Propulsion Laboratory (JPL) ASTER Spectral library (Baldridge et al., 2009), and (2) USA Geological Survey (USGS) Spectral Library (Kokaly et al., 2017). All candidate reference spectra were convolved to Landsat 8 OLI wavelength in the software package ENVI (Harris Geospatial Solutions, Boulder, CO). Candidate image spectra, including GV, NPV and Soil, were extracted by drawing representative region of interest (ROI) polygons in the Landsat imagery and including all pixels in the polygons. Image spectra identified through applying Pixel Purity Index (PPI) were also included. The Coastal Band (Band 1) of all candidate spectra was discarded before further processing.

Combining all candidate reference and image spectra, we identified subsets of spectra from the library through Endmember Optimization module in Viper Tools, an ENVI add-on module (Roberts et al., 2007). For each bright endmember type (GV, NPV and Soil), the spectra with the lowest Endmember Average Root-mean-square-error (EAR; Dennison & Roberts, 2003), lowest Mean Average Spectral Angle (MASA; Dennison et al., 2004) and highest Count-Based Endmember Selection (COB; Roberts et al., 2003) score were selected. In the case of

a tie with COB, EAR was used to split the tie. We consider this subset a reasonable balance between MESMA processing time and endmember variabilities.

We then used this comprehensive endmember set to unmix the selected Landsat OLI imagery. Physically reasonable ranges were set to [0,1] for bright endmembers (GV, NPV and Soil) fractions. The allowed range for Shade fractions was [0, 0.8]. The most complex endmember combinations were four-endmember models (4-EM; three bright EMs plus Shade). All combination sets (2-EM, 3-EM and 4-EM; Table 2) were tested for each pixel, and the one that generated the lowest root-mean-square-error (RMSE) was selected as the candidate model. If this RMSE was no higher than 0.025, the candidate model was selected, otherwise
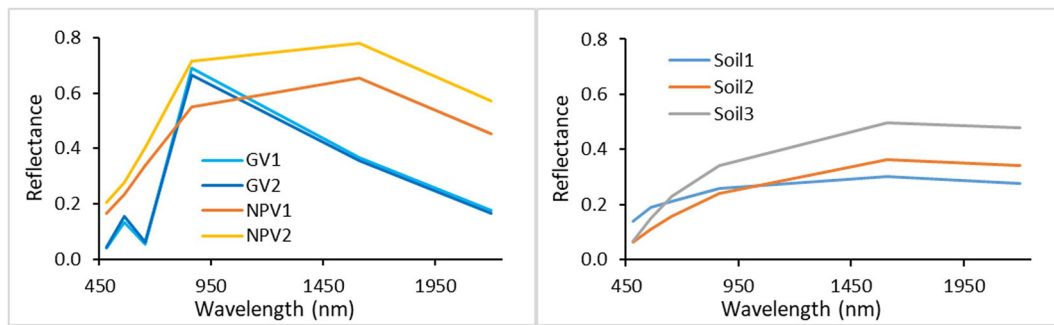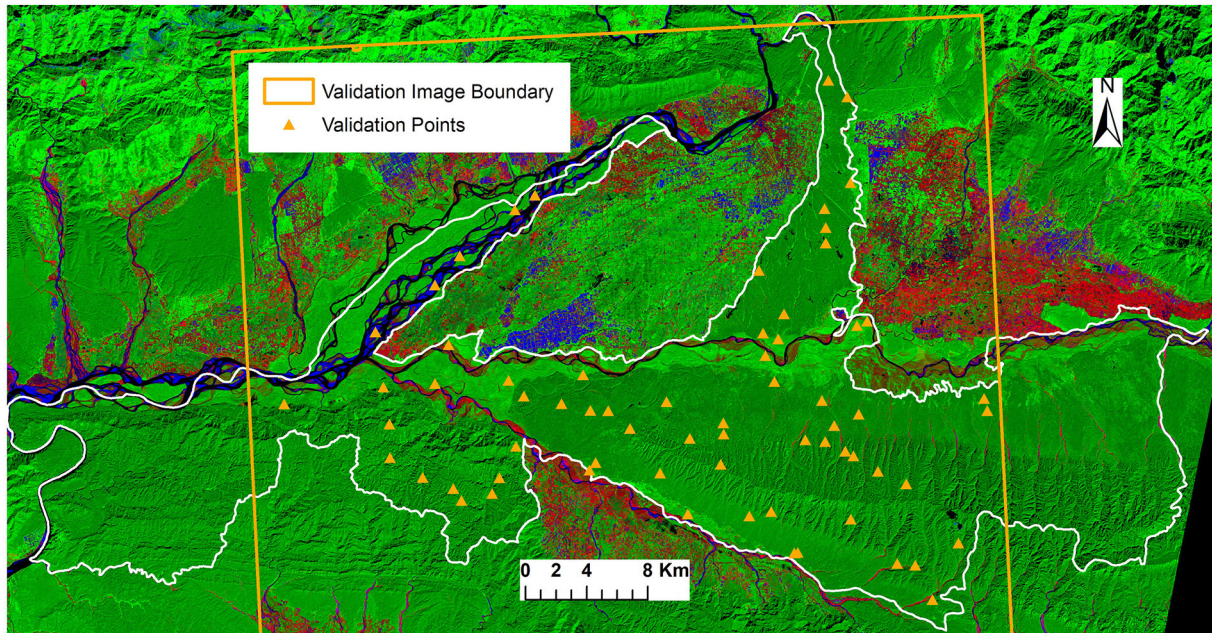
Fig. 4. Spectra included in the final endmember library.

Fig. 5. False colour three band composite of MESMA results with CNP and buffer zone boundaries highlighted (white polygon). Image acquisition date: 27 October 2014. Red: NPV; Green: GV; Blue: Soil; Black: water, cloud, cloud shadow or no data. The southern boundary of the validation image extends beyond this figure extent. The 67 validation points reside within both the study area and validation image boundaries. (For interpretation of the references to colour in this figure legend, the reader is referred to the web version of this article.)
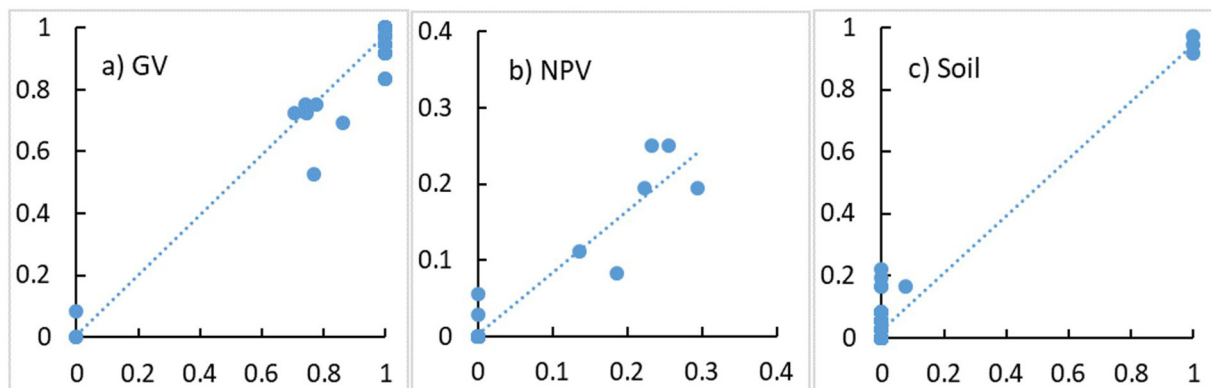

Fig. 6. Scatterplots of MESMA fraction validations.

the pixel was left unmodeled.

For Landsat multispectral imagery of vegetated landscapes, most pixels can be modeled as GV-NPV-Soil-Shade mixture in MESMA. In our study area, *M. micrantha* is genetically and physiologically distinct from other plants, including the other two major invasive species, *Chromolaena odorata* and *Lantana camara*. *M. micrantha* is a perennial creeping vine with higher spectral reflectance than mature forests in the near-infrared wavelength, tends to form dense layers and fill the gaps among top canopies. We hypothesized that the pixels representing areas invaded by *M. micrantha* would yield higher GV fractions and lower Shade fractions than unaffected pixels. To test this hypothesis, we conducted two-sample *t*-tests (two-tailed and unequal variance) for
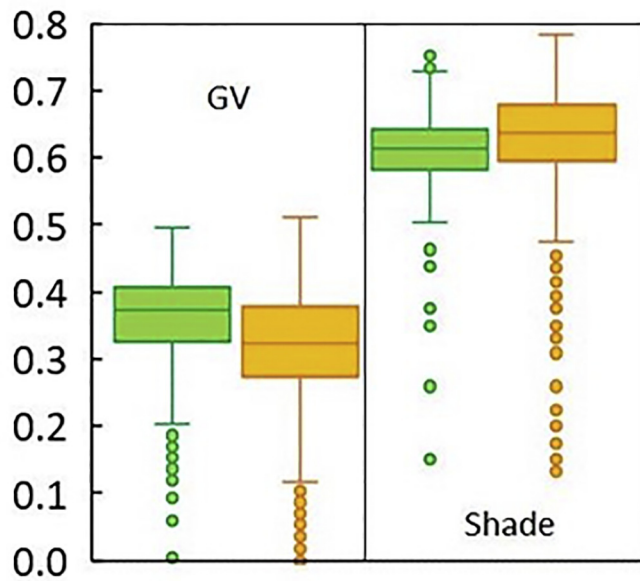
Fig. 7. Boxplots of GV and Shade fractions between presence (green) and community forest background (orange) pixels. (For interpretation of the references to colour in this figure legend, the reader is referred to the web version of this article.)

both GV and Shade fraction values between presence and background pixels to identify potential significant differences.

2.6. Maximum entropy modeling framework

We utilized the software package Maxent to generate models for mapping *M. micrantha* distribution in the Landsat image we selected (Phillips et al., 2006). Maxent makes presence predictions based on the relationships between presence records and corresponding environmental data. The difference between Maxent and many other species distributions modeling methods is that there is no real "absence data" in the modeling procedures, and it is typically developed to accommodate presence-only data. In our vegetation survey, the presence and coverage of *M. micrantha* were recorded for all 5 m by 5 m sample plots. If *M. micrantha* was not detected in a specific sample plot, we cannot guarantee if it was absent from the whole 30 m by 30 m Landsat ground resolution element, or whether the plant was present in that element but outside of the sample plots. Therefore, instead of interpreting the field records as "presence-absence" data, we consider them to be more appropriately treated as "presence-only" data.

We also emphasize the importance of the representativeness of presence data to Maxent model results. The ultimate objective of Maxent is to make predictions of species distributions by evaluating the presence records and their corresponding environmental information, and the representativeness of any presence data is vital to the overall model accuracy. Ideal presence records should include all types of possible presence locations (in the dimensions of the environment data) in the target predicting area. In our research, although the community forests and sample sites are spatially biased, residing mostly on the fringe of the park and covering relatively small areas compared to the whole study area, they were highly diverse in floral species and contained all local vegetation types (e.g. Sal forest, riverine forest and riparian grassland), and consequently contain all possible *M. micrantha* presence location types. Because we are aware of the general distribution pattern of *M. micrantha* in the study area (mostly in riverine habitats), we consider our sampling data to be sufficient.

In the Maxent models, we used the pixels with *M. micrantha* coverage level of 1 or above (excluding all pixels without detected coverage) as presence data; 10,000 pixels were randomly selected from the

study area as background data (Phillips and Dudik, 2008). We imported the four fraction layers (GV, NPV, Soil and Shade, from MESMA) and elevation as potential predictor variables. The maximum iterations were set at 500 times and the predicted *M. micrantha* presence probabilities were averaged for each pixel. The presence data and MESMA fraction layers can only account for the ground conditions around the time the records and imagery were collected, thus for each year (2013, 2014 and 2015), we generated one map for each predictor combination (e.g. GV-Shade-NPV, GV-Shade-Soil and GV-Shade-DEM).

2.7. Model validation

2.7.1. MESMA fraction validation

We obtained a 5-m spatial resolution RapidEye image captured on Nov 29, 2013 to generate reference data and validate the fractions of bright endmembers (e.g. GV, NPV and Soil) in MESMA results. We assumed that since the imagery type and MESMA procedures were consistent among the 3 years (2013–2015), the validation of 1 year's image would be sufficient. MESMA fractions were first shade-normalized before validation. We then generated 100 random points in the study area, and the corresponding pixels were assigned as candidate validation pixels. After excluding points that fell out of the reference image or points where pixels were not modeled by MESMA (e.g. water, cloud, shadow, etc.), 67 pixels were left for validation. Through unsupervised classification in ERDAS and with the aid of Google Earth high spatial-resolution imagery, we classified the reference image into GV, NPV, Soil and other cover types, including water, cloud and shadow. For each bright endmember type (GV, NPV and Soil), using the centroid of the 67 validation pixels as the focal points, we analyzed the focal statistics (sum) at a neighborhood setting of 6 by 6 cells (30 m by 30 m). In this way, the sum divided by 36 would be the reference fraction of that pixel. In the end, validation pixels were assessed using R^2 derived from plotting MESMA fractions (y) against reference fractions (x).

2.7.2. Maxent validation

The receiver operating characteristic (ROC) analysis and the area under the ROC curve (AUC) incorporated in Maxent were used for model evaluation (Fielding and Bell, 1997; Pearce and Ferrier, 2000). AUC values between 0.7 and 0.8 indicate fair modeling results, values between 0.8 and 0.9 are considered good, and values higher than 0.9 are excellent (Fielding and Bell, 1997; Pearce and Ferrier, 2000). We randomly allocated 75% of the presence data for model training, and the remaining 25% for testing. We also applied kappa analysis to evaluate Maxent results (Cohen, 1960). For this purpose, we randomly selected 100 presence pixels and another 100 background pixels from the whole study area in each year's modeling results. Continuous presence probabilities were dichotomized to 0 or 1, with values greater than 0.5 assigned to the latter. Since all pixels, including presence data, were involved in the random selection of background data, the AUC and kappa values tend to be underestimated in this case. Jackknife analyses were conducted to evaluate the relative contributions of the environmental variables. The results are the AUC values of the relative Maxent model if only one of the variables was included in the modeling process (e.g. GV-only or Shade-only Maxent models, etc.).

3. Results

3.1. M. micrantha presence in the sample sites

The fieldwork was conducted in the 2-month window right after the monsoon and it took us 3 years (2013–2015) to survey all 21 community forests. We were able to visit 2219 sample sites in total, of which 1038 were invaded by *M. micrantha*. The four East Sal forests were sparsely invaded, with *M. micrantha* presence at around 10% of the sample sites (Table 3; Fig. 3). Invasions were more prominent in riverine forests, where *M. micrantha* occurred in more than half of the
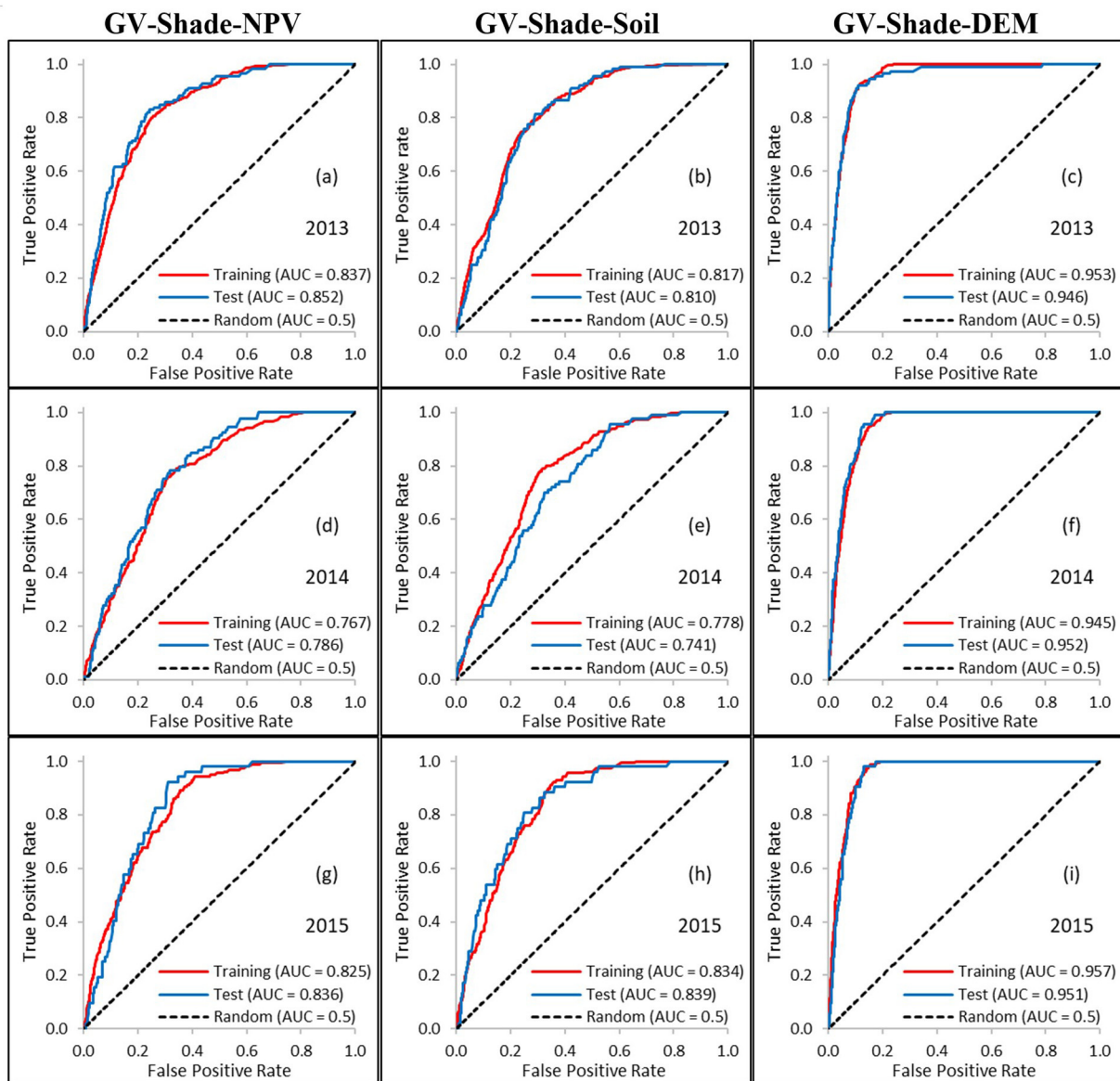
Fig. 8. ROC curves and AUC values for training and test data in GV-Shade-NPV (first column, a, d, g), GV-Shade-Soil (second column, b, e, h) and GV-Shade-DEM (third column, c, f, i) Maxent models for 2013, 2014 and 2015.

sample sites (Table 3; Fig. 3). This general pattern resembles the results from the assessment of *M. micrantha* distribution conducted in the study area in 2008 (Murphy et al., 2013). Forests in the South West Rapti region and the North Narayani region bore the most severe invasion, with invasion rates close to or above 80%. Two forests in particular, MALI and RADH, had *M. micrantha* detected at every sample site.

3.2. MESMA library and fractions

The final endmember library was processed based on the criteria described in Section 2.5 and included two GV (one reference, GV1, and one image, GV2) endmember, two NPV (one reference, NPV1, and one image, NPV2) endmember, and three Soil (two reference Soil2 and Soil3, and one image, Soil1) endmember spectra (Fig. 4). The allowed models consisted of all possible permutations of the endmember types listed in Table 2, resulting in 7 two-endmember models, 16 three-endmember models and 12 four-endmember models (Table 2).

MESMA results without shade normalization are shown in Fig. 5. Water, cloud and shadow were mostly unmodeled and appear black in the map. The park and its buffer zone community forests were

dominated by green vegetation, which included highland Sal forests, riverine forests, and riparian grasslands (Fig. 5). Sal forests accounted for the majority of the green vegetation in the study area, and they appeared darker in the map than the latter two vegetation types. NPV and Soil pure pixels were rare and their fractions were mostly concentrated in riverine habitats, including gravels fields, river banks and senesced grasses. The landscape was observed to be relatively uniform within the study area compared to outside human settlements surrounded by the Narayani and Rapti Rivers, where human settlements and agricultural lands prevailed (Fig. 1). MESMA fraction validation produced a similar range of accuracy for GV ($R^2 = 0.95$), NPV ($R^2 = 0.92$) and Soil ($R^2 = 0.93$), indicating good MESMA results (Fig. 6).

We used the 2219 sample sites in the community forests to identify potential significant differences in GV and Shade fractions between *M. micrantha* invaded sites (1038) and background sites (1181). t-test results confirmed that compared to background pixels, presence pixels generated significantly higher GV fractions and lower Shade fractions (both $p < 0.001$; Fig. 7).
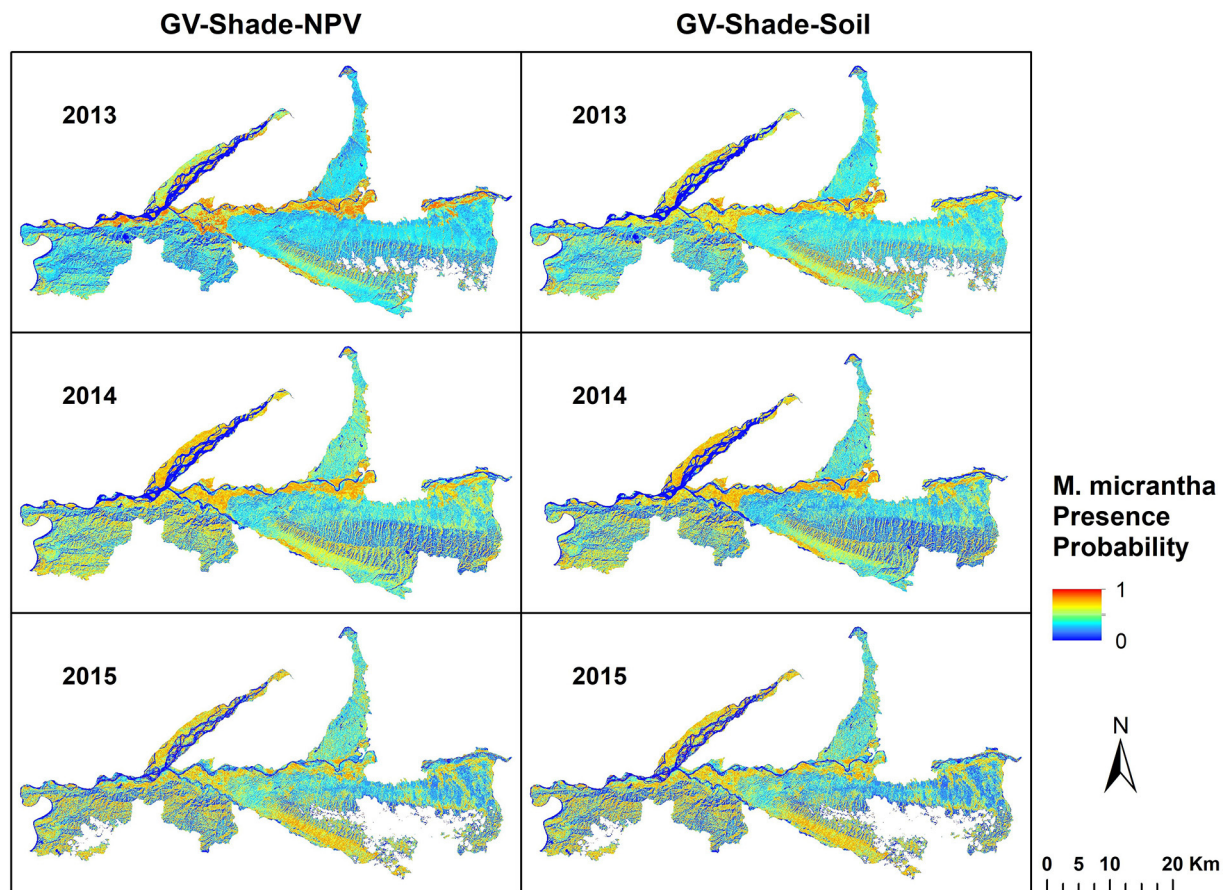
GV-Shade-NPV   **GV-Shade-Soil**

Fig. 9. *M. micrantha* average presence probability maps generated from GV-Shade-NPV (First column from left) and GV-Shade-Soil (Second column from left) Maxent models in 2013, 2014 and 2015. Large blue patches above Churia Hills in 2013 and 2015 maps are associated with clouds or cloud shadows. (For interpretation of the references to color in this figure legend, the reader is referred to the web version of this article.)
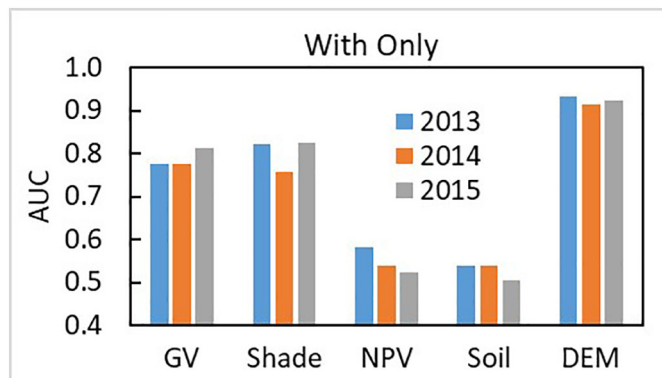

Fig. 10. AUC values of Maxent models with only one of the predictors.

3.3. M. micrantha distribution

Incorporating both GV and Shade fraction layers with an addition of NPV or Soil, the AUC values of *M. micrantha* distribution Maxent models for training and testing data were both between 0.74 and 0.86, respectively (Fig. 8, first two columns from the left). The relative kappa coefficients ranged from 0.49 to 0.61. Both ranges, even though underestimated due to the inclusion of presence records in background data, indicate fair or good model results. The estimated *M. micrantha* presence probabilities ranged from 0 to 1 across the study area, with most of the higher probability pixels located in riverine forests and riparian grasslands along the Narayani and Rapti Rivers (Fig. 9). Some of

the high probabilities were associated with high-GV-fraction pixels at higher elevations, e.g. the sunlit slopes along the southern side of Churia Hills (Fig. 9).

Although MESMA-fraction-only Maxent models (e.g. GV-Shade-Soil and GV-Shade-NPV) produced fair/good model results (AUC between 0.7 and 0.9, kappa between 0.4 and 0.75), the inclusion of elevation (DEM) as a model input significantly improved map accuracy, with both training and testing AUC values around 0.95 (Fig. 8, last column at right). Their kappa coefficients ranged between 0.75 and 0.81. Both ranges indicate excellent mapping results. The effects of including elevation will be further examined in the Discussion section.

4. Discussion

4.1. MESMA fractions and M. micrantha mapping

In this study, we developed an effective approach for mapping understory invasive plant species using SMA and the Maxent modeling framework. By applying MESMA to Landsat 8 OLI surface reflectance products, we verified the significant differences in GV and Shade fractions between *M. micrantha*-invaded and non-invaded pixels. We then successfully mapped the spatial extent of *M. micrantha* in Chitwan National Park and the community forests within its buffer zone using MESMA generated fraction layers. The resulting distribution maps proved to be fair/good for MESMA-fraction-only models (AUC between 0.7 and 0.9, kappa between 0.4 and 0.75). The inclusion of elevation as a model input produced excellent map results (AUC above 0.9 and kappa above 0.75). While endmember fractions from MESMA have been used for sub-pixel land cover mapping (Roberts et al., 1998;
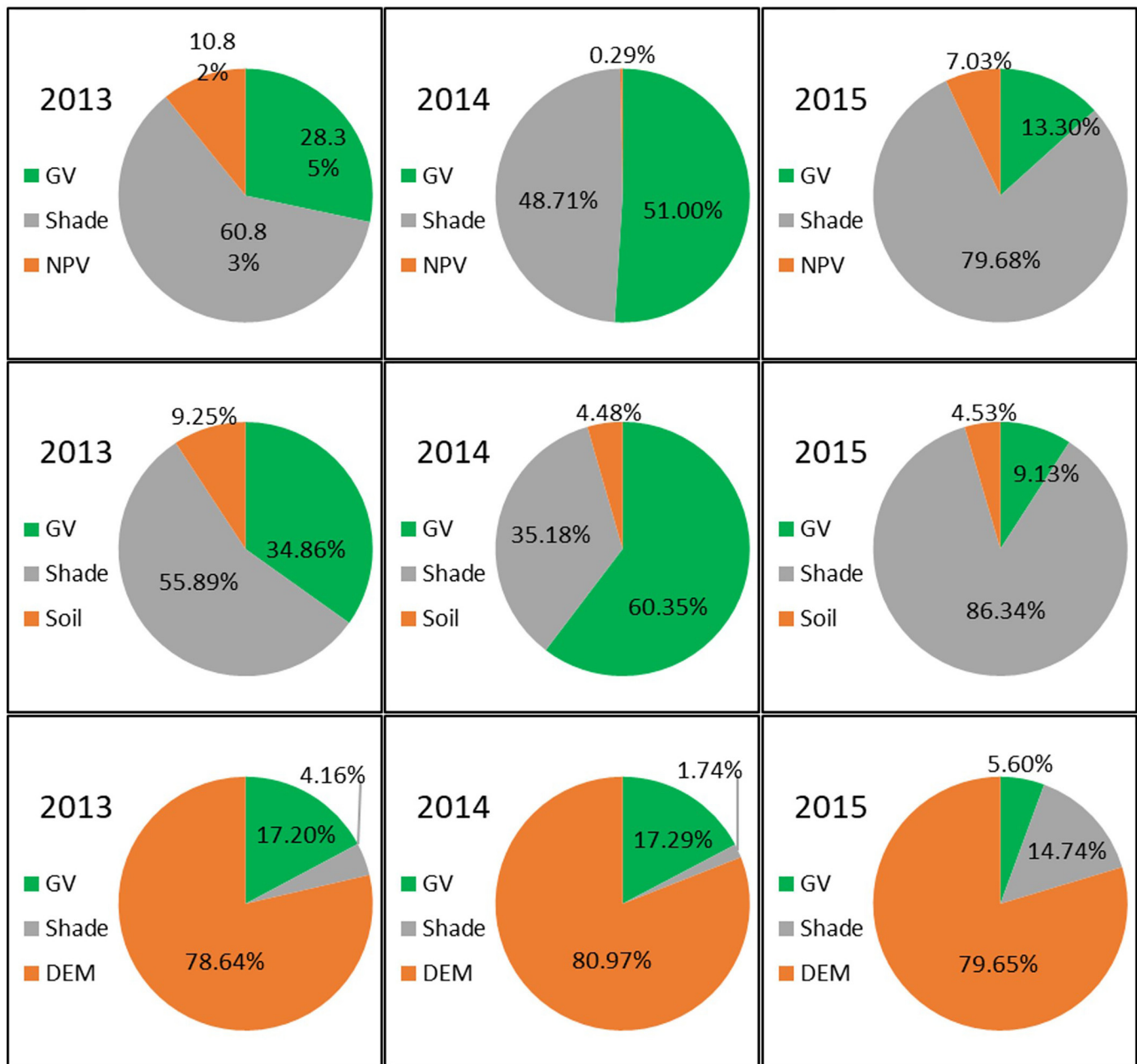
Fig. 11. Predictors' contributions to their relevant Maxent models.

Powell et al., 2007), deforestation and forest degradation evaluation (Souza Jr. et al., 2005; Souza Jr. et al., 2013) and plant species classification (Roberts et al., 2015; Roth et al., 2015), in this study their application was extended to analyze the spatial extent of invasive plant species growing under forest canopies.

By analyzing endmember fractions generated from MESMA, we found that pixels with *M. micrantha* invasion can be distinguished from background pixels in the study area. Higher GV fractions and lower Shade fractions reflect the differences between invaded forests and unaffected landscape types. The growth and densification of *M. micrantha* from ground to tree crowns in the forests may contribute to the higher GV fractions, whereas the filling between canopy gaps may account for the lower Shade fractions of the invaded pixels.

Some of the pixels along the southern side of Churia Hills were also assigned high-probability values, especially in the 2015 maps (Fig. 9). These results might be explained by the limitation of the 2015 presence data, since no Sal forest was sampled that year and all *M. micrantha*

presence records were in riverine forests along the Narayani River (Fig. 2). In addition, due to sun-sensor geometry, sunlit slope vegetation usually has higher reflectance and higher GV values before shade normalization in MESMA. Since the GV fraction was positively related to *M. micrantha* presence, sunlit slope vegetation pixels with high GV values could be assigned with higher presence probabilities. Despite fair model results, the presence data may not be sufficiently representative for predicting sites with distinct environmental conditions in the study area.

4.2. Incorporating elevation

In MESMA-fraction-only Maxent models (e.g. GV-Shade-NPV and GV-Shade-Soil), GV and Shade made prominent contributions to *M. micrantha* mapping, producing fair or good mapping results for both training and test datasets (Fig. 8). Nevertheless, according to the jack-knife analysis in Maxent, although GV and Shade fractions were fair or
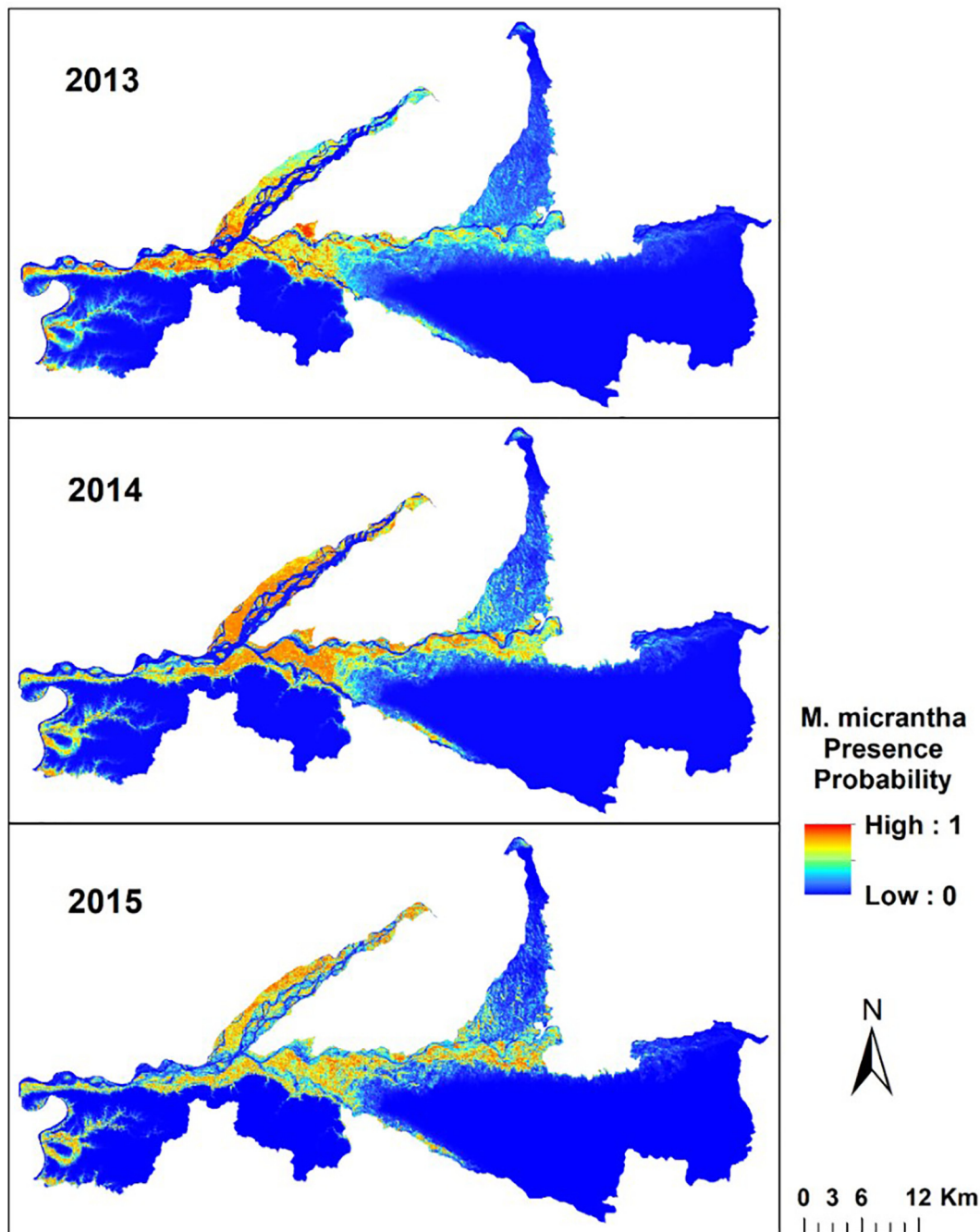
Fig. 12. *M. micrantha* presence probability maps from GV-Shade-DEM Maxent models.

good indicators of understory *M. micrantha* distribution (with-only AUC around 0.8), the most powerful predictor was elevation (with-only AUC above 0.9; Fig. 10). All GV-Shade-DEM Maxent models generated excellent map accuracies (AUC around 0.95; Fig. 8c, f & i), and the contributions of elevation dwarfed that of GV or Shade (Fig. 11). Map results show that the general distribution pattern is similar to those from fraction-only models, with *M. micrantha* presence allocated to pixels close to the Narayani and Rapti Rivers (Fig. 12). However, higher-elevation pixels were mostly assigned with low presence probabilities. This observation is in agreement with local knowledge that most *M. micrantha* was detected in riverine mixed forests, while invasion was less common in higher-elevation Sal forests.

Although elevation made prominent contributions to the map results and it alone could generate excellent model outputs (With-only AUC above 0.9, Fig. 10), both MESMA fractions and elevation are critical in generating optimal *M. micrantha* distribution maps. Elevation alone may have produced good results for our training/testing dataset, which are the sample sites within the community forests, but it may not be sufficient for mapping the whole study area. If elevation was the sole environmental layer, Maxent would assign high presence probabilities to all pixels with low elevation values, such as rivers and lakes (Fig. 13). Landscape factors like elevation may not be sufficient to explain ecological questions such as the distribution of certain species, thus biological factors should also be included. In our case, as indicators of forest structure and canopy conditions, the MESMA fractions were incorporated to produce optimal map results.

4.3. M. micrantha invasion in Chitwan

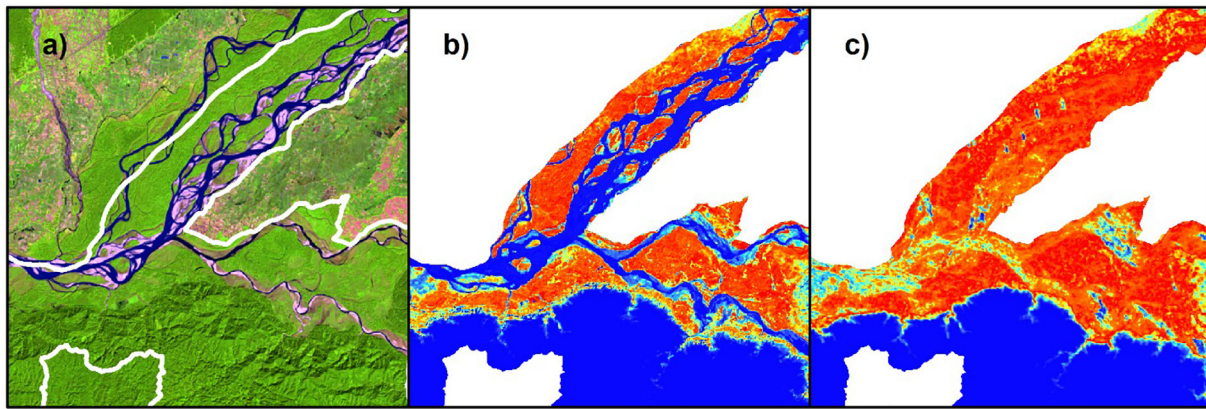Invasion ecology proposes that there are three main steps in the

Fig. 13. (a) depicts a subset of Fig. 1 where the Rapti River joins the Narayani River. Difference between GV-Shade-DEM (b) and DEM-only (c) Maxent models show that DEM-only models assigned high presence probabilities to non-vegetated pixels, including rivers and lakes.

spread of an invasive species: first, an individual or a small population is transported from its native habitat to a geographically distant location it would otherwise not have reached through natural dispersal; secondly, this individual or population survives and reproduces in the new environment and forms sustainable communities; third, the exotic species thrives in the new environment and expands to its immediate neighbors or to more distant areas with the help of environmental or anthropogenic factors such as natural disasters and the movement of animals or humans (Lockwood et al., 2013). *M. micrantha* was introduced from the tropical and subtropical Americas to India in World War II as camouflage for military facilities (Tiwati et al., 2005). It was first reported in eastern Nepal in the early 1960s and reached Chitwan in the early 1990s through catastrophic flooding according to local knowledge. *M. micrantha* is a fast-growing climber which can reproduce through sexual (seeds) or asexual (stems) processes, and its seeds are adapted to fire (Murphy et al., 2013). The stems and seeds of *M. micrantha* would first arrive at and inhabit riverine and riparian environments. After establishing sustainable populations and communities, it would invade higher-elevation habitats that are further away from rivers. In this case, proximity to a river would be the determining factor of the first wave of *M. micrantha* invasion. Besides, *M. micrantha* prefers and grows best in high soil moisture conditions (Zhang and Wen, 2009). It is more likely to invade and thrive in low-lying areas having higher soil moisture. Our results show that by the year 2015, *M. micrantha* invasion in Chitwan National Park and its buffer zone community forests had mostly occurred in riverine forests and riparian grasslands.

4.4. Combination of MESMA and Maxent

In addition to the good agreement between the presence records and the *M. micrantha* distribution maps generated in this study, our approach of combining MESMA and Maxent species distribution modeling provides a novel approach for mapping understory vegetation. In situations where direct detection with satellite data is obscured by canopy tops, Maxent modeling enables understory mapping through indirect methods. Compared to other indirect detection approaches which require additional temporal information through time series analysis of vegetation phenology, our approach only need the process of a single-time image (Tuanmu et al., 2010). Other than the presence records, the only other data we need is remotely sensed which are open source and can be acquired conveniently from online sources. Besides, this approach can be easily extended to other understory plant species, as long as they introduce composition (e.g. GV and Shade fractions) changes alongside their growth.

5. Conclusions

It can be challenging to identify and map understory invasive plants through traditional remote sensing techniques due to the obstruction by canopies. In this paper, we developed an effective and practical approach for mapping understory invasive plant using endmember fractions derived from Landsat 8 OLI imagery and the Maxent modeling framework. The easy access, global coverage and rich historical archive of Landsat data make this approach applicable to a wide range of different study sites. It can also be applied to other satellite imagery with moderate/coarse spatial resolution and global coverage, such as Sentinel 2 data. The combination of MESMA and Maxent provides a significant opportunity for understanding understory vegetation distribution, not only about invasive non-native species, but also native shrubs and herbaceous species. The map results can provide guidance to local invasive plant eradication practices and conservation plans, substantially contributing to ecological restoration, biodiversity conservation, and provision of sustainable ecosystem services in protected areas.

Credit author statement

Conceptualization, data curation, formal analysis: J.D.; Fudning acquisition: L.A., S.J.H., S.T.Y., and J.D.; Supervision: D.A.R., D.A.S., and L.A.; Validation, visualization, writing - original draft: J.D.; Writing - review & editing: J.D., D.A.R., D.A.S., L.A., S.J.H., S.T.Y., and P.C.K.

References

Asner, G.P., Vitousek, P.M., 2005. Remote analysis of biological invasion and biogeochemical change. Proc. Natl. Acad. Sci. 102, 4383–4386.

Asner, G.P., Knapp, D.E., Kennedy-Bowdoin, T., Jones, M.O., Martin, R.E., Boardman, J., Hughes, R.F., 2008. Invasive species detection in Hawaiian rainforests using airborne imaging spectroscopy and LiDAR. Remote Sens. Environ. 112, 1942–1955.

Baldridge, A., Hook, S., Grove, C., Rivera, G., 2009. The ASTER spectral library version 2.0. Remote Sens. Environ. 113, 711–715.

Barbosa, J.M., Asner, G.P., Martin, R.E., Baldeck, C.A., Hughes, F., Johnson, T., 2016. Determining subcanopy *Psidium cattleianum* invasion in Hawaiian forests using imaging spectroscopy. Remote Sens. 8, 33.

Bradley, B.A., 2014. Remote detection for invasive plants: a review of spectral, textural and phenological approaches. Biol. Invasions 16, 1411–1425.

Bradley, B.A., Curtis, C.A., Fusco, E.J., Abatzoglou, J.T., Balch, J.K., Dadashi, S., Tuanmu, M., 2018. Cheatgrass (*Bromus tectorum*) distribution in the intermountain Western USA and its relationship to fire frequency, seasonality, and ignitions. Biol. Invasions 20, 1493–1506.

Central Bureau of Statistics-Nepal, 2011. VDC Wise Population and Households Numbers. Retrieved from. https://cbs.gov.np/ on December 30, 2019.

Charnley, S., Poe, M.R., 2007. Community forestry in theory and practice: where are we now? Annu. Rev. Anthropol. 36, 301–336.

Cohen, J., 1960. A coefficient of agreement for nominal scales. Educ. Psychol. Meas. 20, 37–46.

Critical Ecosystem Partnership Fund (CEPF), 2019. Retrieved from. http://www.cepf.net/resources/hotspots/Asia-Pacific/Pages/Himalaya.aspx.

Dennison, P.E., Roberts, D.A., 2003. Endmember selection for multiple endmember spectral mixture analysis using endmember average RMSE. Remote Sens. Environ. 87, 123–135.

Dennison, P.E., Halligan, K.Q., Roberts, D.A., 2004. A comparison of eror metrics and constraints for multiple endmember spectral mixture analysis and sepctral angle mapper. Remote Sens. Environ. 93, 359–367.

Fielding, A.H., Bell, J.F., 1997. A review of methods for the assessment of prediction errors in conservation presence/absence models. Environ. Conserv. 24, 38–49.

Hoyos, L.E., Gavier-Pizarro, G.I., Kuemmerle, T., Bucher, E.H., Radeloff, V.C., Tecco, P.A., 2010. Invasion of glossy privet (*Ligustrum lucidum*) and native forest loss in the Sierres Chicas of Cordoba, Argentina. Biol. Invasions 12, 3261–3275.

International Union for Conservation of Nature (IUCN), 2019. 100 of the World's Worst Invasive Alien Species. http://www.iucngisd.org/gisd/100_worst.php.

Joshi, C., De Leeuw, J., van Andel, J., Skidmore, A.K., Lekhak, H.D., van Duren, I.C., Norbu, N., 2006. Indirect remote sensing of a cryptic forest understory invasive species. For. Ecol. Manag. 225, 245–256.

Kokaly, R.F., Clark, R.N., Swayze, G.A., Livo, K.E., Hoefen, T.M., Pearson, N.C., Wise, R.A., Benzel, W.M., Lowers, H.A., Driscoll, R.L., Klein, A.J., 2017. USGS Spectral Library Version 7: U.S. Geological Survey Data Series 1035. 61 p. https://doi.org/10.3133/ds1035.

Lishawa, S.C., Treering, D.J., Vail, L.M., McKenna, O., Grimm, E.C., Tuchman, N.C., 2013. Reconstructing plant invasions using historical aerial imagery and pollen core analysis: *Typha* in the Laurentian Great Lakes. Divers. Distrib. 19, 14–28.

Lockwood, J.L., Hoopes, M.F., Marchetti, M.P., 2013. Invasion Ecology. Wiley-Blackwell, Hoboken, NJ.

McCormick, C.M., 1999. Mapping exotic vegetation in the Everglades from large-scale aerial photographs. Photogramm. Eng. Remote. Sens. 65, 179–184.

Murphy, S.T., Subedi, N., Jnawali, S.R., Lamichhane, B.R., Upadhyay, G.P., Kock, R., Amin, R., 2013. Invaisve mikania in Chitwan National Park, Nepal: the threat to the greater one-horned rhinoceros *Rhinoceros unicornis* and factors driving the invasion. Oryx 47, 361–368.

Nagendra, H., 2002. Tenure and forest conditions: community forestry in the Nepal Terai. Environ. Conserv. 29 539.

NASA/METI/AIST/Japan Spacesystems, U.S./Japan ASTER Science Team, 2019. ASTER Global Digital Elevation Model V003 [Data set]. NASA EOSDIS Land Processes DAAChttps://doi.org/10.5067/ASTER/ASTGTM.003. Accessed 2019-12-30 from.

Pearce, J., Ferrier, S., 2000. Evaluating the predictive performance of habitat models developed using logistic regression. Ecol. Model. 133, 225–245.

Pearlstine, L., Portler, K.M., Smith, S.E., 2005. Textural discrimination of an invasive plant, *Schinus terebinthifolius*, from low altitude aerial digital imagery. Photogramm. Eng. Remote. Sens. 71, 289–298.

Pejchar, L., Mooney, H.A., 2009. Invasive species, ecosystem services and human wellbeing. Trends Ecol. Evol. 24, 497–504.

Peterson, E.B., 2005. Estimating cover of an invasive grass (*Bromus tectorum*) using tobit regression and phenology derived from two dates of Landsat ETM+ data. Int. J. Remote Sens. 26, 2491–2507.

Phillips, S., Dudik, M., 2008. Modeling of species distributions with Maxent: new extensions and a comprehensive evaluation. Ecography 31, 161–175.

Phillips, S., Anderson, R., Schapire, R., 2006. Maximum entropy modeling of species geographic distributions. Ecol. Model. 190, 231–259.

Powell, R.L., Roberts, D.A., Dennison, P.E., Hess, L.L., 2007. Sub-pixel mapping of urban land cover using multiple endmember spectral mixture analysis: Manaus, Brazil. Remote Sens. Environ. 106, 253–267.

Roberts, D.A., Smith, M.O., Adams, J.B., 1993. Green vegetation, nonphotosynthetic vegetation, and soils in AVIRIS data. Remote Sens. Environ. 44, 255–269.

Roberts, D.A., Gardner, M., Church, R., Ustin, S., Scheer, G., Green, R., 1998. Mapping chaparral in the Santa Monica Mountains using multiple endmember spectral mixture models. Remote Sens. Environ. 65, 267–279.

Roberts, D.A., Dennison, P.E., Gardner, M.E., Hetzel, Y., Ustin, S.L., Lee, C.T., 2004. Evaluation of the potential of Hyperion for fire danger assessment by comparison to the Airborne Visible/Infrared Imaging Spectrometer. IEEE Transactions on Geoscience and Remote Sensing 41, 1297–1310.

Roberts, D.A., Halligan, K., Dennison, P.E., 2007. VIPER Tools User Manual. Visualization and Image Processing for Environmental Research Laboratory, Department of Geography, University of California, Santa Barbara.

Roberts, D.A., Dennison, P.E., Roth, K.L., Dudley, K., Hulley, G., 2015. Relationships between dominant plant species, fractional cover and land surface temperature in a Mediterranean ecosystem. Remote Sens. Environ. 167, 152–167.

Roth, K.L., Roberts, D.A., Dennison, P.E., Alonzo, M., Peterson, S.H., Beland, M., 2015. Differentiating plant species within and across diverse ecosystems with imaging spectroscopy. Remote Sens. Environ. 167, 135–151.

Somers, B., Asner, G.P., 2013. Multi-temporal hyperspectral mixture analysis and feature selection for invasive species mapping in rainforests. Remote Sens. Environ. 136, 14–27.

Souza Jr., C.M., Roberts, D.A., Cochrane, M.A., 2005. Combining spectral and spatial information to map canopy damage from selective logging and forest fires. Remote Sens. Environ. 98, 329–343.

Souza Jr., C.M., Siqueira, J.V., Sales, M.H., Fonseca, A.V., Ribeiro, J.G., Numata, I., Cochrane, M.A., Barber, C.P., Roberts, D.A., Barlow, J., 2013. Ten-year Landsat classification of deforestation and forest degradation in the Brazilian Amazon. Remote Sens. 5, 5493–5513.

Spiteri, A., Nepal, S., 2008. Distributing conservation incentives in the buffer zone of Chitwan National Park, Nepal. Environ. Conserv. 35, 76–86.

Taylor, S.L., Hill, R.A., Edwards, C., 2013. Characterizing invasive non-native Rhododendron ponticum spectra signatures with spectroradiometry in the laboratory and field: potential for remote mapping. ISPRS J. Photogramm. Remote Sens. 81, 70–81.

Tiwati, S., Adhikari, B., Siwakoti, M., Subedi, K., 2005. An Inventory and Assessment of Invasive Alien Plant Species of Nepal. IUCN, Kathmandu, Nepal.

Tuanmu, M., Vina, A., Bearer, S., Xu, W., Ouyang, Z., Zhang, H., Liu, J., 2010. Mapping understory vegetation using phenological characteristics derived from remotely sensed data. Remote Sens. Environ. 114, 1833–1844.

Underwood, E., Ustin, S., DiPietro, D., 2003. Mapping nonnative plants using hyperspectral imagery. Remote Sens. Environ. 86, 150–161.

United Nations Educational, Scientific and Cultural Organization (UNESCO), 2019. World Heritage List. Retrieved from. http://whc.unesco.org/en/list/284.

Wilfong, B.N., Gorchow, D.L., Henry, M.C., 2009. Detecting an invasive shrub in deciduous forest understories using remote sensing. Weed Sci. 57, 512–520.

Zhang, L.L., Wen, D.Z., 2009. Structural and physiological responses of two invasive weeds, *Mikania micrantha* and *Chromolaena odorata*, to contrasting light and soil water conditions. J. Plant Res. 122, 69–79.